Limestone calcination at Calcium-Looping conditions for CO_2 capture and Thermochemical Energy Storage in the presence of H_2O: In-situ XRD analysis.

Jose Manuel Valverde[a], Santiago Medina[b]

[a] Faculty of Physics. University of Seville. Avenida Reina Mercedes s/n, 41012 Sevilla, Spain

[b] X-Ray Laboratory (CITIUS), University of Seville,

Avenida Reina Mercedes, 4B. 41012 Sevilla, Spain

Abstract

This work reports an in-situ XRD analysis on the calcination/carbonation behavior of natural limestone ($CaCO_3$) as affected by the addition to the calciner of H_2O at a very small concentration under relevant Calcium-Looping (CaL) conditions for CO_2 capture in coal fired power plants (CFPP) and Thermochemical Energy Storage (TCES) in Concentrated Solar Power plants (CSP). Previous studies have demonstrated that the presence of steam in the calciner at high concentration yields a significant increase of the reaction rate. However, a further undesired consequence is the serious deterioration of the CaO mechanical strength, which would lead to particle attrition and mass loss in any CaL process based on the use of circulating fluidized beds. Results presented in this manuscript on the time evolution of the wt% and crystallite size of the phases involved in the calcination/carbonation reactions indicate that the calcination rate is still notably increased by the presence of H_2O at very small concentrations whereas the reactivity toward carbonation and crystal structure of the formed CaO are not essentially affected, which suggests that neither the CaO mechanical strength is impaired. Thus, the benefit of using steam for calcination in the CaL process could be still retained while at the same time particle attrition would not be promoted.

I. INTRODUCTION

The calcination/carbonation reaction of limestone ($CaCO_3$)

$$CaCO_3 \leftrightarrows CaO + CO_2(g) \quad \Delta_r H^0 = +177.8\text{kJ/mol} \tag{1}$$

lies at the heart of a vast number of industrial applications and natural processes. This reaction plays an important role in the production of building materials, iron and steel, fertilizers, food processing, disinfection, water treatment, desulphurization, plastics, glass, sugar refining, pharmaceutics, etc. As a result, it has been one of the most widely investigated gas-solid heterogeneous reactions despite of which the physicochemical mechanisms behind it are not fully understood yet [1–8].

Generally, some relevant properties of the CaO derived from calcination are its porosity, reactivity, crystal structure and mechanical strength, which are critically determined by the environmental conditions under which the reaction evolves. Thus, archaeological studies show that the calcination of limestone or dolomite ($CaMg(CO_3)_2$) in ancient Roman ovens was carried out under high CO_2 concentration to produce deterioration resistant and high mechanical strength mortar [9]. Recently, limestone and dolomite calcination under superheated steam at reduced temperatures has become a commercial technology to produce enhanced CaO and MgO based fertilizers and cement products with a higher reactivity, low crystallinity and high friability [10]. Heat conductivity of the gases present in the calciner environment and CO_2 diffusivity has long been identified as critical physical properties that greatly influence the kinetics of calcination [11, 12]. Thus, the calcination rate of limestone is significantly increased at reduced temperatures under Helium (with a rather high thermal conductivity and CO_2 diffusivity as compared to air) without any significant effect on the structure and reactivity of the produced CaO [13]. Similarly, calcination is significantly promoted under superheated steam at high concentrations, which was originally attributed to the enhancement of thermal conductivity in the calciner atmosphere [12] although more recent works suggest that H_2O plays a critical catalytic role on $CaCO_3$ decomposition [14]. As a consequence of such chemical action, crystallinity, mechanical strength and reactivity

of the resulting CaO are fundamentally affected [10, 11, 15]. The enhancement of CaO sintering and crystallite size growth as due to the presence of H_2O in the calciner environment at high concentration is a well known effect widely reported in the literature [16–20].

Recent studies [6, 21] have shown that limestone calcination is initiated by a topotactical chemical decomposition of $CaCO_3$ into a metastable CaO^* phase, which subsequently transforms into the stable CaO form lime. Accordingly, the reaction mechanism would consist of a two steps process:

1. **Chemical decomposition**

$$CaCO_3 + L \rightleftarrows CaO^* + L(CO_2)$$

2. **Desorption/structural transformation**

$$CaO^* + L(CO_2) \rightleftarrows CaO + L + CO_2(g)$$

Here L represents an active site in the solid where calcination occurs, $L(CO_2)$ denotes a molecule of CO_2 that remains physically adsorbed after chemical decomposition. The CaO^* metastable phase appears as a pseudomorph from calcite ($CaCO_3$) before the stable form lime (CaO) nucleates [6]. Figure 1 shows the crystallographic unit cells of the three phases ($CaCO_3$ calcite, CaO^*, and CaO lime) that would be expectedly involved in the calcination reaction [6, 21]. The hexagonal rhombohedral calcite structure (space group $R\overline{3}c$, 167) yields after chemical decomposition a cubic metastable CaO^* structure (space group $Fm\overline{3}m$, 225) as a dilated pseudomorph of lime (same space group that CaO^*) which appears afterwards.

On the other hand, thermochemical data shows that the relationship between the CO_2 partial pressure P in the calcination atmosphere and temperature T for the reaction to be at equilibrium is given by [16, 22, 23]

$$P \approx A \exp(-20474/T) \tag{2}$$

where $A = 4.134 \times 10^{12}$ Pa. In regards to kinetics, experimental measurements at high CO_2 partial pressures near the equilibrium partial pressure show a significant slow down of the reaction [8, 24]. Under these conditions, calcination is severely hindered by CO_2 desorption and the exothermicity of the $CaO^* \rightarrow CaO$ transformation step, which makes it necessary to increase the calciner temperature well above the equilibrium temperature (or, equivalently, increase P_{eq}) for the reaction to occur sufficiently fast in applications wherein the calciner is operated under high CO_2 partial pressure [24]. If the concentration of CO_2 in the calcination environment is not high, the CO_2 desorption and structural transformation step occurs extremely fast and does not limit the reaction kinetics [6, 21].

A. The Calcium Looping process

In the past few years the Calcium-Looping (CaL) process, based on the cyclic calcination/carbonation of limestone, has come onto scene with a high potential to mitigate CO_2 emissions. The integration of the CaL process into coal fired power plants has been already successfully demonstrated at the pilot scale (1-2 MW_{th}) level [25–27]. In this process (Fig. 2a), early proposed by Shimizu et al. [28], the CO_2 loaded flue gas ($\sim$ 15% CO_2 vol concentration) is used to fluidize a bed of CaO particles at temperatures around 650°C , which leads to fast carbonation of the CaO solids. The carbonated particles are then circulated into a second reactor wherein CaO is regenerated by calcination at temperatures typically close to $\sim$ 950°C . CO_2 concentration in the calciner must be necessarily high in order to extract it as pure as possible for compression and the subsequent storage. For this reason, the

calciner temperature has to risen well over the equilibrium temperature, which is $T \simeq 896°C$ under pure CO_2 at atmospheric pressure. To this end, a practical solution is to burn fuel in the calciner using pure O_2 (oxy-combustion), albeit this method poses a significant energy penalty to the process [29]. Moreover, additional CO_2 is released by oxy-combustion and the reactivity of the regenerated CaO is drastically impaired due to enhanced sintering under high temperatures/high CO_2 concentration [17], deactivation by ashes and irreversible sulphation [25].

A further emerging application of the CaL process is Thermochemical Energy Storage (TCES) in Concentrated Solar Power (CSP) plants, which was proposed in the late 1970s [30] but still remains at the concept stage [31, 32]. Remarkably, the calcination/carbonation conditions under which the solids would be cycled in the CaL-CSP integration to maximize the global efficiency differ radically from those used in the CaL process for CO_2 capture. Thus, according to a recently proposed integration scheme [32], carbonation in the CaL-CSP integration would be carried out at high temperatures ($>\sim 850°C$) under high CO_2 partial pressure whereas the solids would be preferably calcined in the solar receiver at the lowest possible temperature in order to reduce technological risks and cost by using commercial metallic receivers (Fig. 2b). Electricity would be produced on demand in a gas turbine by the CO_2 in excess over the stoichiometric ratio not used for carbonation and carrying the heat of this exothermic reaction. Solar energy would provide the heat for the endothermic calcination reaction, which could be performed at a fast enough rate at temperatures around 725°C by using He or superheated steam in the calciner [33].

The use of steam in diverse ways has been widely studied in the last years to improve the CaL performance for CO_2 capture [15, 25, 34–38]. Thus, it has been observed that the intermediate hydration of CaO at relatively low temperatures ($\sim$200 - 400°C), with

the formation of $Ca(OH)_2$, leads to a significant reactivation of the sorbent [25, 34, 35, 38]. Nevertheless, the mechanical strength of the hydrated sorbent is severely impaired, which causes the generation of very fine particle fragments by attrition that cannot be recovered and are therefore lost, thus negating the benefit of reactivation. The multicycle CaO activity can be also enhanced by the presence of steam (at vol % typically in the range 5 - 40%) in the carbonator and/or the calciner [15, 36, 37]. Experimental observations show that steam in the calciner leads to the formation of large yet relatively stable pores thus mitigating CaO deactivation with the number of cycles [15, 37]. On the other hand, some studies have shown a relevant increase of the calcination rate in the presence of H_2O at high concentration [11, 12, 14, 39]. It has been suggested that CO_2 desorption would be enhanced by the more favorable adsorption of H_2O, which would catalyze in this way the calcination reaction [14]. H_2O dynamic adsorption/desorption was already proposed as the driving mechanism for calcination under H_2O in the early works of Anderson et al. [18, 40]. Atomistic simulations analysis of CO_2/H_2O co-adsorption in CaO crystal surfaces show a preference of H_2O adsorption over CO_2 adsorption [41–43], which agrees with previously reported UPS and XPS measurements [44]. The efficiency of the CaL process in both CO_2 capture and TCES applications would benefit notably from a reduction of the calcination temperature. Nevertheless, a detrimental side effect of calcination under steam is a reduction of the mechanical strength of the resulting CaO solids. MacIntire and Stansel [11] early observed that limes derived from calcination in steam were exceedingly pulverous as demonstrated by their decidedly greater tendencies to remain in suspension. Promoted fracturing of the particles resulting from calcination under steam is also reported in the recently developed Catalytic Flash Calcination (CFC) Technology [10].

The energy efficiency of the CaL process would benefit notably from a reduction of the

calcination temperature [29] as might be achieved by the use of steam albeit the enhancement of particle fracturing would be a drawback. In the work reported in the present manuscript, we tested the presence of steam at very small concentration in the calciner on the rate of limestone calcination and CaO reactivity by means of in-situ XRD analysis. This study served us also to investigate the crystal structure of the formed CaO, which is closely related to its mechanical strength. As will be seen, the use of steam at very small concentrations in the calciner still leads to a significant reduction of the minimum temperature to achieve full calcination in short residence times without causing any relevant change on neither the structure nor the reactivity of the resulting CaO.

II. EXPERIMENTAL MATERIAL AND METHODS

In this work we have used a powdered natural limestone of high purity (99.6% $CaCO_3$) from Matagallar quarry (Pedrera, Spain). Volume weighted mean particle size is 9.5 μm as measured by laser diffractometry (Malvern Mastersizer 2000 instrument). Thus, the influence of intra-particle diffusion resistance on the reaction rate, which would be relevant only for particle sizes above $\sim$300 μm [23, 45], can be neglected.

In situ XRD tests have been carried out by means of the experimental setup depicted in Fig. 3. The powder sample of mass around 150 mg is placed over a 0.01 m diameter porous ceramic plate inside the reaction chamber, which is operated at atmospheric pressure. A controlled gas flow is passed at the same rate in all the runs (1000 scc/min) downwards and across the powder, which facilitates a homogeneous distribution of the gas in the powder thus promoting gas-solid contacting efficiency and mass/heat transfer. Pure N_2, He and CO_2 are employed under dry and wet conditions to test the sample calcination behavior. H_2O was added to the dry gas by bubbling the gas flow in distilled water at ambient temperature

using a SYCOS H (Ansyco, Germany) accurate humidity controller, which yields a H_2O vol. concentration in the wet gas of 0.03%. For calcination tests under N_2 and He, the temperature was increased at a rate of 10°C /min from ambient to 725°C as representative of conditions to be expected in the CaL process for CSP energy storage. XRD scans during the temperature ramps were registered each 25°C at constant temperature in the range $20° < 2\theta < 60°$ (0.03°/step, step time of 0.2 s and tube conditions of 40 kV and 40 mA). On the other hand, for calcination tests under CO_2 , the temperature was increased up to reach a target calcination temperature above 900°C as corresponding to CaL conditions for CO_2 capture. This high temperature was kept constant for a given time period while XRD scans were continuously recorded as calcination evolved. Additionally, the carbonation behavior of the samples was tested in-situ readily after calcination. To this end, the temperature was set to 850°C and CO_2 was introduced in the reaction chamber after which XRD scans were continuously registered as carbonation evolved.

In situ XRD analysis has been carried out by means of a Bruker D8 Advance powder diffractometer provided with a fast response/high sensitivity detector (Bruker Vantec 1), radial Soller slits and 60 mm Gobel mirrors (Bruker, Germany). Cu K_α radiation (0.15405 nm wavelength) has been employed with parallel Johansson geometry in the incident beam. The instrument is equipped with an Anton Paar XRK 900 high temperature chamber specially designed for high temperature gas-solid reactions. Dead volumes are avoided to achieve a homogeneous filling with the reaction gas and temperature gradients across the sample are minimized. The temperature of the sample is accurately measured by means of a pair of NiCr/NiAl thermocouples placed close to the sample holder. Corundum, LaB_6 and silicon standards were employed in a wide range of diffraction angles to correct instrumental contributions for structural adjustments and resolution. The recorded XRD scans were analyzed

by using the software TOPAS 5 (Bruker) [46], which allowed us to accurately obtain the wt% and coherent crystal length (crystallite size) of the different phases involved in the reaction by means of Rietveld refinement [47] and Le Bail methods [48], respectively. Rietveld and Le Bail refinements were performed using the fundamental parameters method. Zero error (2θ), sample displacement, and absorption and lattice parameters of the phases were allowed to vary in order to search for the best fittings. The background was fitted by a fourth-order Chebychev polynomial. Lorentz and polarization geometric factors for the measurement configuration were used. The crystallite sizes were calculated using the best combinations of Gaussian and Lorentzian functions. The robustness of the data derived was checked from the values of several fitting indicators such as the goodness-of-fit and residual factors (Rwp and RBragg) [47].

III. RESULTS AND DISCUSSION

Figure 4a shows the time evolution of $CaCO_3$ wt% during the calcination tests carried out under dry N_2 and He atmospheres. As reported in previous works [12, 13, 33], it is seen that the calcination rate is significantly enhanced under dry He as compared to N_2, which can be explained by the notably higher thermal conductivity and CO_2 diffusivity in He. The thermal conductivity of He at temperatures around 700°C is $\lambda \simeq$350 mW/(m K) [49] whereas it is $\lambda \simeq$60 mW/(m K) [49] for N_2. On the other hand, because of the very low He molecular weight, CO_2 diffusivity in He is rather high ($D \simeq 0.7 \times 10^{-2}$ m^2/s at atmospheric pressure and room temperature) as compared to CO_2 diffusivity in N_2 ($D \simeq 0.16 \times 10^{-2}$ m^2/s). These values would increase with the 1.5 to 1.8 power of temperature [50]. Thus, the remarkable enhancement of heat and mass transfer when calcination is carried out under He would allow it to occur at a faster rate. In our tests we observe that calcination is

completely attained at 700°C under He whereas the temperature must be further increased about 25°C to achieve full calcination under N_2. On the other hand, as seen in Fig. 4a, the rate of carbonation of the CaO resulting from calcination is not influenced by the type of gas, either He or N_2, under which calcination was performed.

The time evolution of $CaCO_3$ wt% during calcination tests carried out under N_2 and He atmospheres under dry and wet conditions is shown in Figs. 4b-c. Interestingly, the presence of H_2O in the calcination atmosphere, even at the very small concentration used in our tests (0.03 vol %), yields a noticeable acceleration of calcination for both gases. Thus, calcination proceeds at a similar rate under wet N_2 than under dry He and becomes almost completed at 700°C . In the case of wet He, the reaction rate is further increased and it is fully attained completely at about 680°C . As may be seen in Figs. 4b-c the presence of H_2O at the small concentration of our tests does not lead to any significant effect on the reactivity toward carbonation of the CaO resulting from calcination. Figures 4b-c show that CaO carbonation occurs through two well differentiated stages as well known from previous studies [27]. A first reaction controlled phase takes place until a $CaCO_3$ layer is built upon the surface of the CaO particles. This stage is rather fast at the carbonation temperature of our experiments and is followed by a much slower phase limited by solid state diffusion of ions across the $CaCO_3$ product layer. The rate of carbonation in the solid-sate diffusion controlled phase is therefore determined by the diffusion coefficient, which mainly depends on the solid crystal structure and the presence of impurities. Thus, the similar carbonation rate observed in our tests of the CaO resulting from calcination under dry and wet conditions (Figs. 4b-c) suggests that the crystal structure of the solids is not affected by the presence of H_2O at the small concentration used in our experiments. This observation is consistent with crystallite size data inferred from the in-situ XRD analysis (Figs. 5a-b). This

suggests that the remarkable influence of H_2O observed on the calcination rate is not due to a catalyzing effect of the H_2O molecules on CO_2 desorption as was suggested in previous works from calcination tests under higher H_2O concentrations. Indeed, such chemical action would have led to a CaO structure with higher reactivity toward carbonation and promoted crystallite size not observed in our tests. Since the CaO crystal structure is not influenced by the small H_2O concentration used in our tests, it might be expected that neither the CaO mechanical strength is compromised as would be the case if calcination was carried out under H_2O at relatively higher concentrations. Although a direct link between crystallinity and mechanical strength cannot be generally established, such correlation has been recently reported elsewhere for the calcium based materials used in our work [51]. Thus, our results suggest that the addition of H_2O at very small concentrations in the calciner would allow in practice reducing further the calcination temperature under He to about 680°C in the CaL process for CSP energy storage without compromising the mechanical strength of the CaO particles resulting for calcination.

Next we analyze the effect of the presence of H_2O in the calciner environment at CaL conditions relevant for CO_2 capture involving calcination under CO_2 at high concentration. Figure 6 shows the time evolution of in-situ XRD patterns continuously recorded for calcination at 925°C under dry and wet CO_2 . As may be seen, the presence of H_2O, despite its very low concentration, has also a significant effect under these conditions. Thus, full decarbonation is achieved after just about 10 min in the case of wet CO_2 calcination whereas it takes more than 30 min to be completed under dry CO_2 . The time evolution of $CaCO_3$ wt% during calcination/carbonation tests carried out under dry and wet CO_2 at different temperatures (903, 911, and 925°C) is plotted in Fig. 7. At the lowest temperature (903°C), which is just 7°C over the equilibrium temperature, calcination under dry CO_2 is not

even started after 2 h. However, the addition of H_2O at the very low vol % used in our tests allows calcination to be initiated after an induction period of about 1.5 h, albeit at a very slow rate. By increasing the temperature to 911°C , calcination is observed to be started after about 70 min under dry CO_2 and proceeds at a very slow pace. At this same temperature, the induction period is shortened to just about 15 min under wet CO_2 and the reaction speed is multiplied by a factor of almost 3. At a temperature of 925°C the reaction speed is increased by a similar factor when H_2O is present in the calcination chamber and calcination becomes fully attained after a few minutes, which is fast enough for practical purposes.

The above observations are consistent with results reported from thermogravimetric analysis and pilot-scale tests indicating that the calciner temperature must be raised to about 950°C under dry conditions and high CO_2 partial pressure to achieve complete calcination in just a few minutes of the fresh limestone makeup that must be periodically introduced in the reactor to counteract CaO deactivation with the number of CaL cycles [26, 27]. Injection of steam in the calciner at relatively high concentrations has been proven in previous works to improve the multicycle stability of the formed CaO [15, 37]. However, the chemical action of steam at high concentrations affects also the CaO structure so as to seriously impair its mechanical strength [11]. As seen in Fig. 7 the carbonation rate in the diffusion limited phase of the CaO formed at the conditions of our tests is not influenced by the presence of H_2O, which suggests that neither the CaO structure is significantly altered under wet CO_2 calcination as compared to dry CO_2 . This is supported by data on the time evolution of $CaCO_3$ and CaO crystallite size showing no significant difference between dry and wet CO_2 calcination (Fig. 8). Thus, we may infer that the presence of H_2O at the small concentration used in our tests leads to a significant acceleration of calcination allowing for a reduction

of the calcination temperature whereas the mechanical strength of the generated CaO is neither impaired at CaL conditions for CO_2 capture. As derived from CaL process simulations within the context of its application for CO_2 capture [29] a reduction of the calciner temperature by just 20°C while maintaining a high calciner efficiency might notably reduce the energy penalty of the technology. Thus, such temperature reduction would allow to cut down the amounts of coal and oxygen needed for oxy-combustion to raise the calciner temperature, which would also diminish the additional CO_2 produced by oxy-combustion. Simulations [29] indicate that the ratio of the mass of coal needed for oxy-combustion to the mass of CO_2 captured could be decreased by a 5% if the calciner temperature could be lowered from 950°C to 930°C. In the ordinary CaL configuration a low calciner to carbonator inventory ratio (of about 0.2) would be only possible by calcination at 950°C (yielding a high calciner efficiency) whereas a decrease of the calciner temperature to 930°C would require increasing this ratio to about 0.4 as the calciner efficiency becomes impaired [29]. Thus, achieving efficient calcination at 930°C by using H_2O at very small concentrations as suggested by our work would serve to reduce significantly the solids inventory in the calciner thus decreasing the energy penalty of the technology.

As discussed above the effect of He on speeding up calcination as compared to N_2 can be explained by the enhancement of thermal transfer and CO_2 diffusivity. These gas physical properties promote the transfer of heat from the furnace to the self-cooling reactant due to the reaction endothermicity and evacuation of the CO_2 released far from the surface of the material. The effect observed in the present work of the addition of H_2O in the calcination environment cannot be certainly attributed to a change of the physical properties of the calciner atmosphere, which would not be sufficiently modified by just a 0.03 vol % H_2O concentration. Moreover, we have seen that calcination is enhanced also under wet He with

a higher thermal conductivity than H_2O (at 700°C the thermal conductivity of H_2O is 90 mW/(m K) [52] whereas it is 350 mW/(m K) for He [49]). The results obtained on the CaO reactivity and crystallite size suggest also that neither H_2O acts chemically by facilitating CO_2 desorption to speed up the CaO^* →CaO structural transformation. In fact, this step has been seen to limit calcination only at conditions near equilibrium and under high CO_2 partial pressure [6, 21]. Thus, it would be relevant in any case only for the tests carried out under pure CO_2 in our work. The presence of the phase CaO^* during calcination under CO_2 may be certainly inferred from a detailed analysis of the XRD patterns recorded for calcination under CO_2 . Figure 9a shows a zoom of an experimentally recorded XRD pattern around 29.1^0 where the main reflection peak of calcite (104) is located for calcination under dry CO_2 at 925°C . As may be observed, the experimentally recorded peak is slightly shifted with respect to the location of the theoretical calcite peak. A better fit is obtained by taking into account the presence of the metastable CaO^* phase, whose main reflection peak (111) is found around 29.3^0. Figure 9b shows the goodness-of-fit parameter for the best Rietveld fits obtained with and without taking into consideration the presence of CaO^* during calcination under dry CO_2 at 925°C . Values of the goodness-of-fit closer to unity, which are indicative of better fits, are systematically obtained when the presence of the metastable CaO^* phase is allowed. CaO^* wt% data calculated during our calcination tests as a function of $CaCO_3$ conversion at diverse temperatures and under dry and wet CO_2 are shown in Fig. 10. As may be seen, CaO^* is detected although at quite low concentrations, and its wt% drops quickly with $CaCO_3$ conversion. Remarkably, for a given calcination temperature the CaO^* wt% evolution only depends on $CaCO_3$ conversion independently of whether calcination is carried out in the presence or absence of H_2O. Thus, the evolution of CaO^* does not seem to be significantly affected by the presence of H_2O at the conditions of our tests despite

the important effect that H_2O has on the reaction kinetics. These results indicate that the fundamental mechanism by which the presence of H_2O at the small concentration used in our tests accelerates calcination is not related to the catalysis of CO_2 desorption and CaO structural transformation, which is consistent with the absence of any effect of H_2O observed above on the reactivity and crystallite size of the CaO that results from calcination.

On the other hand, the effect of H_2O in the calciner at very low concentrations observed in our work could be rationalized from the unconventional physical approach to decomposition of alkaline-earth carbonates proposed by L'vov [4, 53], which has remained largely ignored in the field of thermal analysis. This mechanism assumes that decomposition is initiated by the congruent dissociative evaporation of $CaCO_3$ molecules. The main, rate-limiting stage would be the reaction of volatile $CaCO_3$ with H_2O molecules, which would be present in the reactor environment even under dry conditions at residual concentrations ($<\sim 10^{-4}$ vol %), resulting in the formation of low-volatility $Ca(OH)_2$ as reaction intermediate. $Ca(OH)_2$ vapor would rapidly condensate onto the solid and decompose afterwards into CaO and H_2O. Since condensation of $Ca(OH)_2$ generates heat, part of this heat would go into the excitation of the H_2O molecules released in the decomposition of the solid $Ca(OH)_2$. The activated H_2O molecules would interact more effectively with volatile $CaCO_3$ molecules as compared to inactivated H_2O, therefore accelerating decomposition. The model foresees that a slight excess of H_2O in the reactor over its residual presence under dry conditions would significantly reduce the decomposition temperature [53]. Thus, the significant effect on the calcination kinetics of very low H_2O concentrations (0.03 vol %) observed in our work could find an explanation in this mechanism of intermediate $Ca(OH)_2$ formation. Moreover, this approach predicts that the influence of water vapor in the presence of CO_2 at high concentration on the calcination rate should be further magnified [53], which is consistent also with

our experimental findings. Remarkably, our work is to our knowledge the first experimental report published in the literature showing a relevant effect of very small amounts of water vapor on the kinetics of $CaCO_3$ decomposition as early predicted by Lvov's model. Nevertheless, such mechanism of intermediate hydroxide formation would involve the presence of crystalline $Ca(OH)_2$ as a metastable phase during the transformation [53], which we fail to detect at the conditions of our in-situ XRD tests.

IV. CONCLUSIONS

The CaL process is being widely investigated in the last years for its applications to capture CO_2 from coal fired power plants and thermochemical storage of CSP. In both applications, a reduction of the calcination temperature would greatly contribute to improve energy efficiency. Importantly, the conditions of calcination in both applications are rather diverse although a common requirement is that calcination must be completed in short residence times on the order of several minutes. Thus, calcination in the CaL process for CO_2 capture must be carried out under high CO_2 concentration whereas, in the case of CaL-CSP conditions, calcination would be ideally carried out under a gas separable from CO_2 that would allow at the same time a considerable reduction of the calcination temperature such as He due to its high thermal conductivity and CO_2 diffusivity. Experimental observations reported elsewhere indicate that under these conditions calcination of natural limestone is quickly completed for temperatures around $\sim$950°C and $\sim$ 725°C under CO_2 and He, respectively. Previous studies have also shown that the addition of steam at relatively high concentrations catalyzes calcination. Furthermore, the reactivity of the formed CaO is enhanced albeit the chemical action of H_2O affects critically the CaO crystal structure and impairs severely the CaO mechanical strength, which poses a serious limitation to the

practical use of steam in circulating fluidized beds. The in-situ XRD analysis shown in the present work demonstrates that the use of H_2O at very small concentrations yields still a significant acceleration of the calcination reaction whereas the CaO reactivity and crystal structure are not essentially affected. These results have been obtained at CaL conditions relevant for both CO_2 capture ad CSP energy storage and suggest the possibility of reducing in both applications the calcination temperature by about $\sim$20°C without compromising the mechanical strength of the formed CaO.

V. ACKNOWLEDGEMENTS

This work was supported by the Spanish Government Agency Ministerio de Economia y Competitividad (contract CTQ2014-52763-C2-2-R). We gratefully acknowledge the X-ray service of the Innovation, Technology and Research Center of the University of Seville (CITIUS).

VI. REFERENCES

[1] Boynton, R. S. *Chemistry and Technology of Lime and Limestone;* Wiley: New York, 1980 For general practical information, the interested reader is recommended perusal of the first edition (1966).

[2] Towe, K. M. *Nature* **1978,** *274,* 239 - 240.

[3] Caceres, P.; Attiogbe, E. *Minerals Engineering* **1997,** *10,* 1165 - 1176.

[4] L'vov, B. V.; Polzik, L. K.; Ugolkov, V. L. *Thermochimica Acta* **2002,** *390,* 5 - 19.

[5] Beruto, D.; Searcy, A. W.; Kim, M. G. *Thermochimica Acta* **2004,** *424,* 99 - 109.

[6] Rrodriguez-Navarro, C.; Ruiz-Agudo, E.; Luque, A.; Navarro, A. B.; Ortega-Huertas, M. *American Mineralogist* **2009,** *94,* 578 593.

[7] Michele, P.; Loic, F.; Michel, S. *Thermochimica Acta* **2011,** *525,* 93 - 102.

[8] Valverde, J. M.; Sanchez-Jimenez, P. E.; Perez-Maqueda, L. A. *The Journal of Physical Chemistry C* **2015,** *119,* 1623-1641.

[9] Beruto, D.; Vecchiattini, R.; Giordani, M. *Thermochimica Acta* **2003,** *404,* 25 - 33.

[10] Sceats, M.; Horley, C. "System and method for the calcination of minerals", 2014 US Patent 8,807,993.

[11] MacIntire, W. H.; Stansel, T. B. *Industrial & Engineering Chemistry* **1953,** *45,* 1548-1555.

[12] Berger, E. E. *Industrial & Engineering Chemistry* **1927,** *19,* 594-596.

[13] Valverde, J. M.; Medina, S. *ACS Sustainable Chemistry & Engineering* **2016,** *4,* 7090-7097.

[14] Wang, Y.; Thomson, W. J. *Chemical Engineering Science* **1995,** *50,* 1373 - 1382.

[15] Donat, F.; Florin, N. H.; Anthony, E. J.; Fennell, P. S. *Environmental Science & Technology* **2012,** *46,* 1262 - 1269.

[16] Stanmore, B.; Gilot, P. *Fuel Processing Technology* **2005,** *86,* 1707 - 1743.

[17] Borgwardt, R. H. *Industrial & Engineering Chemistry Research* **1989,** *28,* 493 - 500.

[18] Anderson, P. J.; Horlock, R. F.; Avery, R. G. *Proc. Br. Ceram. Soc.* **1965,** *3,* 33.

[19] Agnew, J.; Hampartsoumian, E.; Jones, J.; Nimmo, W. *Fuel* **2000,** *79,* 1515 - 1523.

[20] Fierro, V.; Adnez, J.; Garcia-Labiano, F. *Fuel* **2004,** *83,* 1733 - 1742.

[21] Valverde, J. M.; Medina, S. *Phys. Chem. Chem. Phys.* **2015,** *17,* 21912-21926.

[22] Barin, I. *Thermochemicaldata of pure substances;* Weinheim: VCH.: 1989.

[23] Garcia-Labiano, F.; Abad, A.; de Diego, L.; Gayan, P.; Adanez, J. *Chemical Engineering Science* **2002,** *57,* 2381 - 2393.

[24] Valverde, J. M. *Chemical Engineering Science* **2015,** *132,* 169–177.

[25] Blamey, J.; Anthony, E. J.; Wang, J.; Fennell, P. S. *Prog. Energ. Combust. Sci.* **2010,** *36,* 260–279.

[26] Hanak, D. P.; Anthony, E. J.; Manovic, V. *Energy Environ. Sci.* **2015,** *8,* 2199-2249.

[27] Perejon, A.; Romeo, L. M.; Lara, Y.; Lisbona, P.; Martinez, A.; Valverde, J. M. *Applied Energy* **2016,** *162,* 787 - 807.

[28] Shimizu, T.; Hirama, T.; Hosoda, H.; Kitano, K.; Inagaki, M.; Tejima, K. *Chemical Engineering Research & Design* **1999,** *77,* 62 - 68.

[29] Martinez, A.; Lara, Y.; Lisbona, P.; Romeo, L. M. *Environmental Science & Technology* **2013,** *47,* 11335-11341.

[30] Flamant, G.; Hernandez, D.; Bonet, C.; Traverse, J.-P. *Solar Energy* **1980,** *24,* 385 - 395.

[31] Edwards, S. E.; Materic, V. *Solar Energy* **2012,** *86,* 2494 - 2503.

[32] Chacartegui, R.; Alovisio, A.; Ortiz, C.; Valverde, J.; Verda, V.; Becerra, J. *Applied Energy* **2016,** *173,* 589 - 605.

[33] Sarrion, B.; Valverde, J. M.; Perejon, A.; Perez-Maqueda, L.; Sanchez-Jimenez, P. E. *Energy Technology* **2016,** *4,* 1013–1019.

[34] Blamey, J.; Manovic, V.; Anthony, E. J.; Dugwell, D. R.; Fennell, P. S. *Fuel* **2015,** *150,* 269 - 277.

[35] Blamey, J.; Paterson, N. P. M.; Dugwell, D. R.; Fennell, P. S. *Energy Fuels* **2010,** *24,* 4605–4616.

[36] Symonds, R. T.; Lu, D. Y.; Manovic, V.; Anthony, E. J. *Industrial & Engineering Chemistry Research* **2012,** *51,* 7177 - 7184.

[37] Champagne, S.; Lu, D. Y.; Macchi, A.; Symonds, R. T.; Anthony, E. J. *Industrial & Engineering Chemistry Research* **2013,** *52,* 2241-2246.

[38] Phalak, N.; Wang, W.; Fan, L.-S. *Chemical Engineering & Technology* **2013,** *36,* 1451–1459.

[39] Asano, K.; Fujimoto, K.; Yamaguchi, Y.; Ito, S. Reactivity of Carbonates in Superheated Steam under Atmospheric Pressure. In *Inorganic and Environmental Materials*, Vol. 617; Trans Tech Publications: 2014.

[40] Anderson, P. J.; Morgan, P. L. *Trans. Faraday Soc.* **1964,** *60,* 930–937.

[41] de Leeuw, N. H.; Watson, G. W.; Parker, S. C. *The Journal of Physical Chemistry* **1995,** *99,* 17219-17225.

[42] Allen, J. P.; Parker, S. C.; Price, D. W. *The Journal of Physical Chemistry C* **2009,** *113,* 8320-8328.

[43] Allen, J. P.; Marmier, A.; Parker, S. C. *The Journal of Physical Chemistry C* **2012,** *116,* 13240 - 13251.

[44] Onishi, H.; Egawa, C.; Aruga, T.; Iwasawa, Y. *Surface Science* **1987,** *191,* 479 - 491.

[45] Grasa, G.; Murillo, R.; Alonso, M.; Abanades, J. C. *AIChE J.* **2009,** *55,* 1246–1255.

[46] Bruker, A. *Bruker AXS GmbH, Karlsruhe, Germany Search PubMed* **2014,** .

[47] (Ed.), R.-A. Y. *The Rietveld Method;* IUCr Monographs on Crystallography 5; Oxford University Press: New York, 1993.

[48] Le Bail, A. *Powder Diffraction* **2005,** *20,* 316–326.

[49] Vargaftik, N. B.; Yakush, L. V. *Journal of engineering physics* **1977,** *32,* 530–532.

[50] Cussler, E. *Diffusion: Mass Transfer in Fluid Systems;* Cambridge Series in Chemical Engineering Cambridge University Press: 1997.

[51] Valverde, J. M.; Sanchez-Jimenez, P. E.; Perez-Maqueda, L. A.; Quintanilla, M.; Perez-Vaquero, J. *Applied Energy* **2014,** *125,* 264 - 275.

[52] Huber, M. L.; Perkins, R. A.; Friend, D. G.; Sengers, J. V.; Assael, M. J.; Metaxa, I. N.; Miyagawa, K.; Hellmann, R.; Vogel, E. *Journal of Physical and Chemical Reference Data* **2012,** *41,* 033102.

[53] L'vov, B. V. *Thermochimica Acta* **1997,** *303,* 161 - 170.

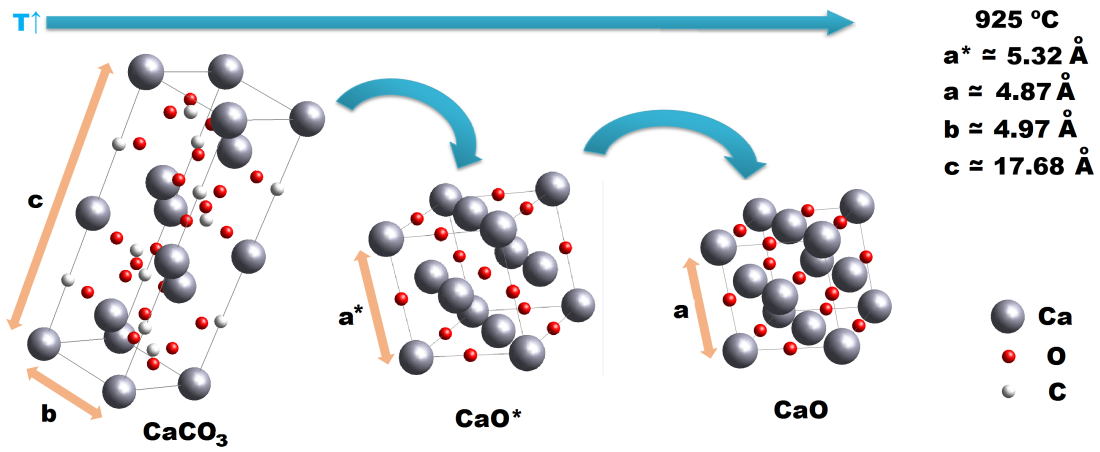

FIG. 1: Transformation during calcination of the hexagonal rhombohedral calcite structure (space group R$\bar{3}$c, 167) into a cubic metastable CaO* structure (space group Fm$\bar{3}$m, 225) as a dilated pseudomorph of the final stable CaO form lime (same space group that CaO*). Cell parameters indicated are calculated for a temperature of 925°C . Adapted from [21].

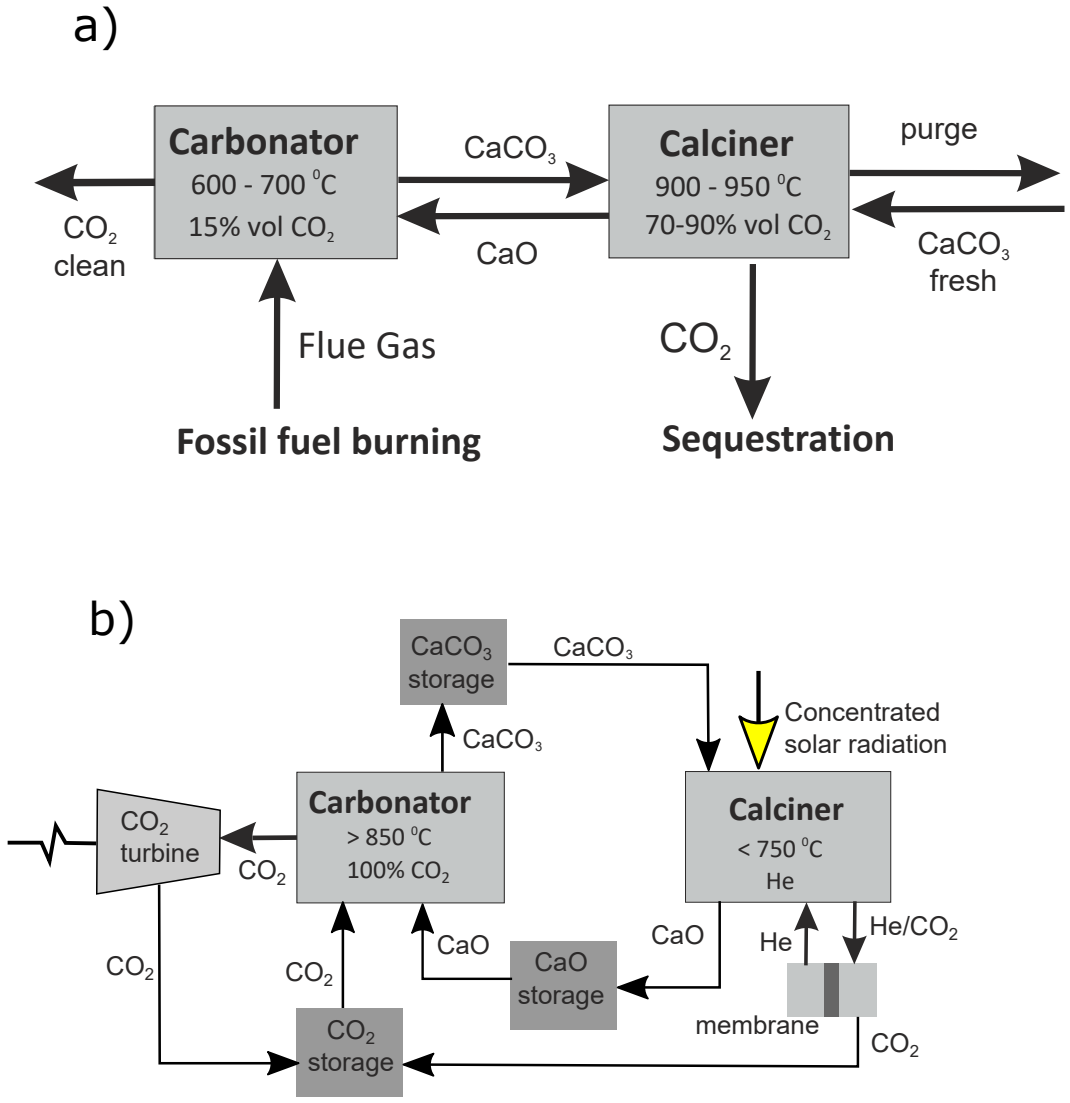

FIG. 2: Flow diagrams of the Calcium Looping process for CO_2 capture in fossil fuel fired power plants (a) demonstrated at the pilot scale (1 - 2 MW_{th}) stage [26] and for Thermochemical Energy Storage in Concentrated Solar Power plants (b) currently at the concept stage [32].

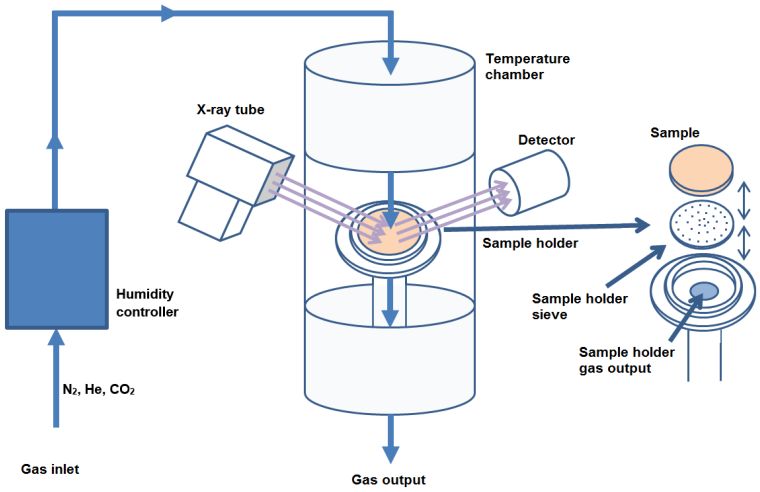

FIG. 3: Schematic layout of the experimental setup used in this work for limestone calcination/carbonation in-situ XRD analysis under different dry and wet gases.

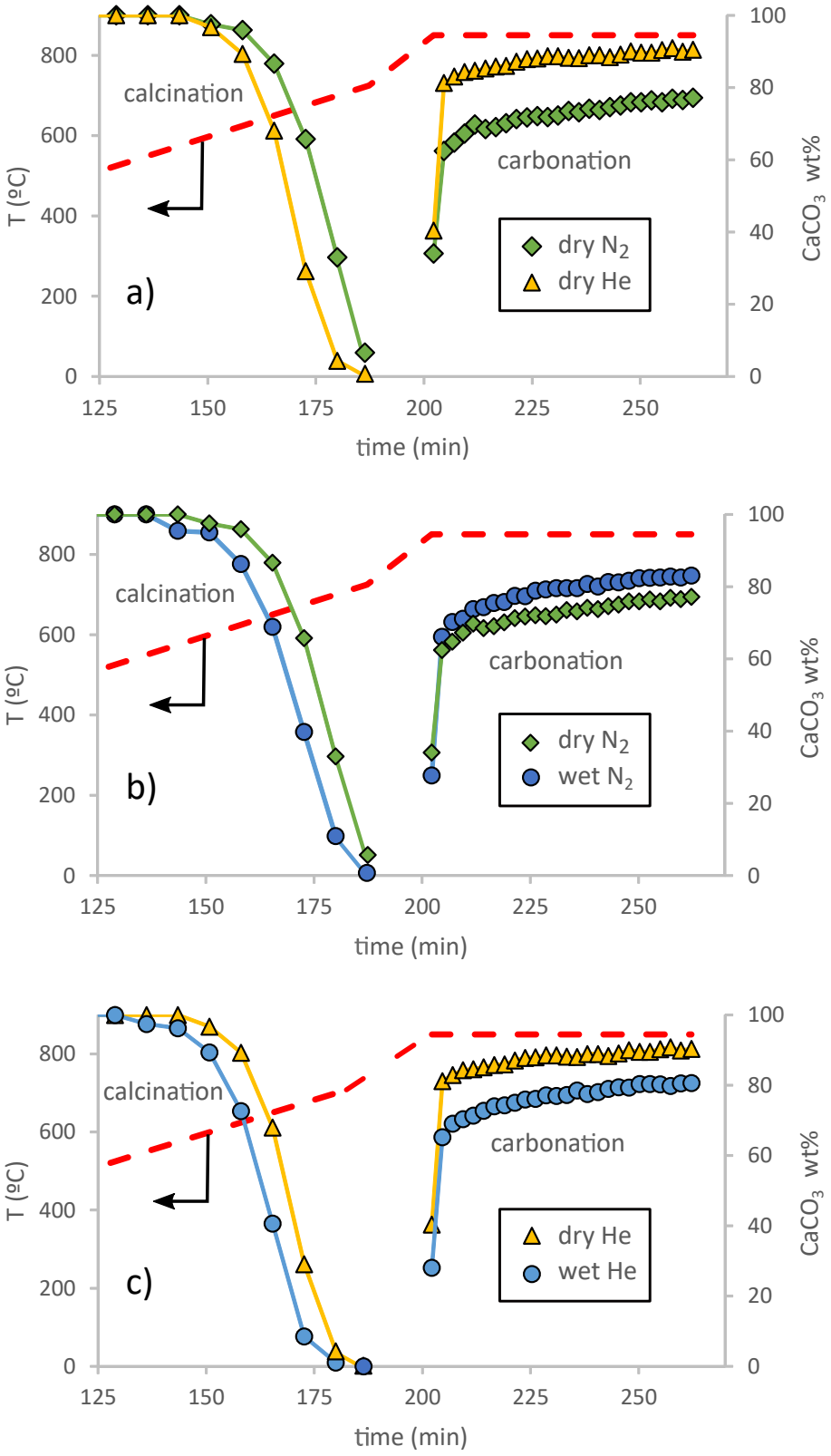

FIG. 4: Time evolution of temperature (left axis) and $CaCO_3$ wt% during calcination/carbonation tests carried out under dry N_2 and He (a), dry and wet N_2 (b) and dry and wet He (c) atmospheres.

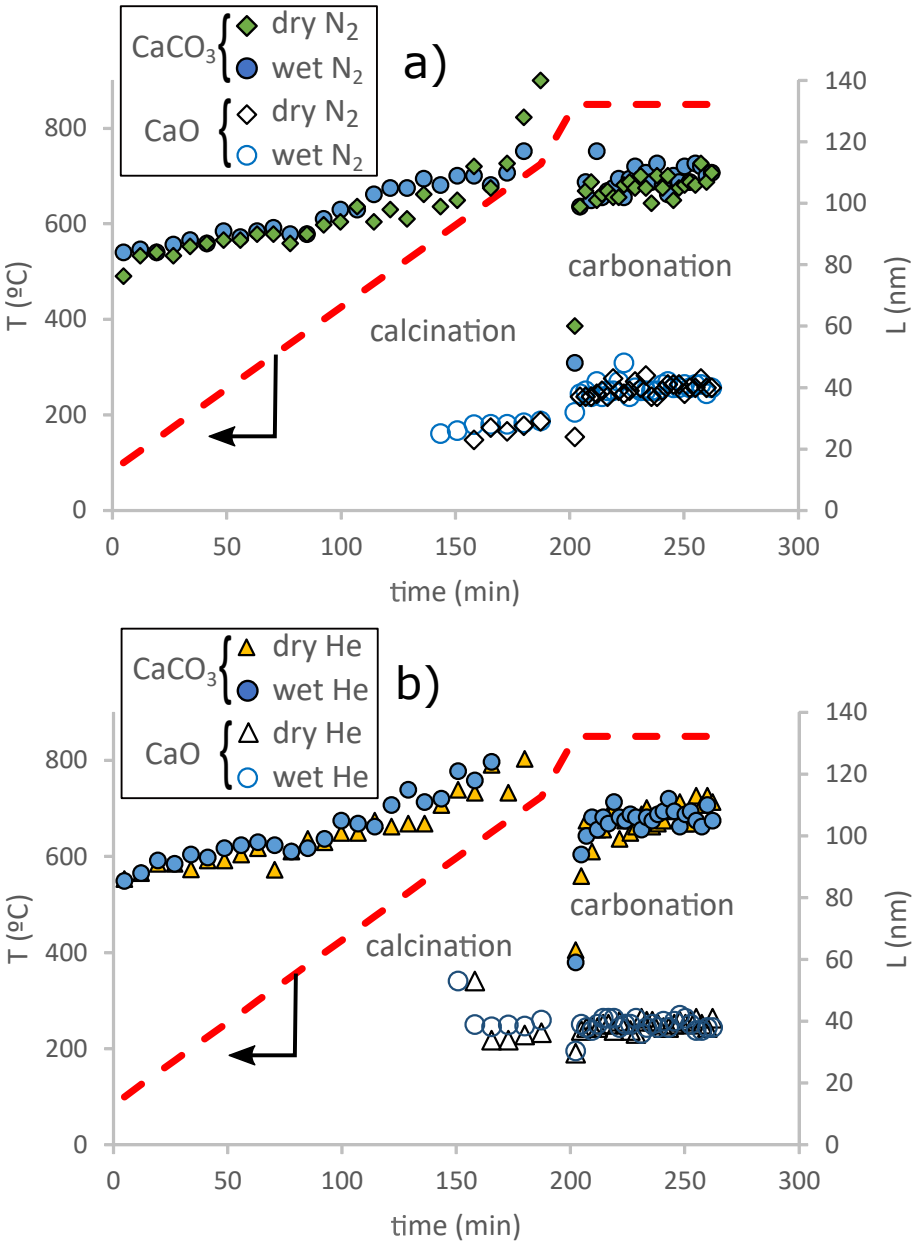

FIG. 5: Time evolution of temperature (left axis) and crystallite size (right axis) of $CaCO_3$ and CaO during calcination/carbonation tests carried out under dry and wet N_2 (a), and dry and wet He (c) atmospheres.

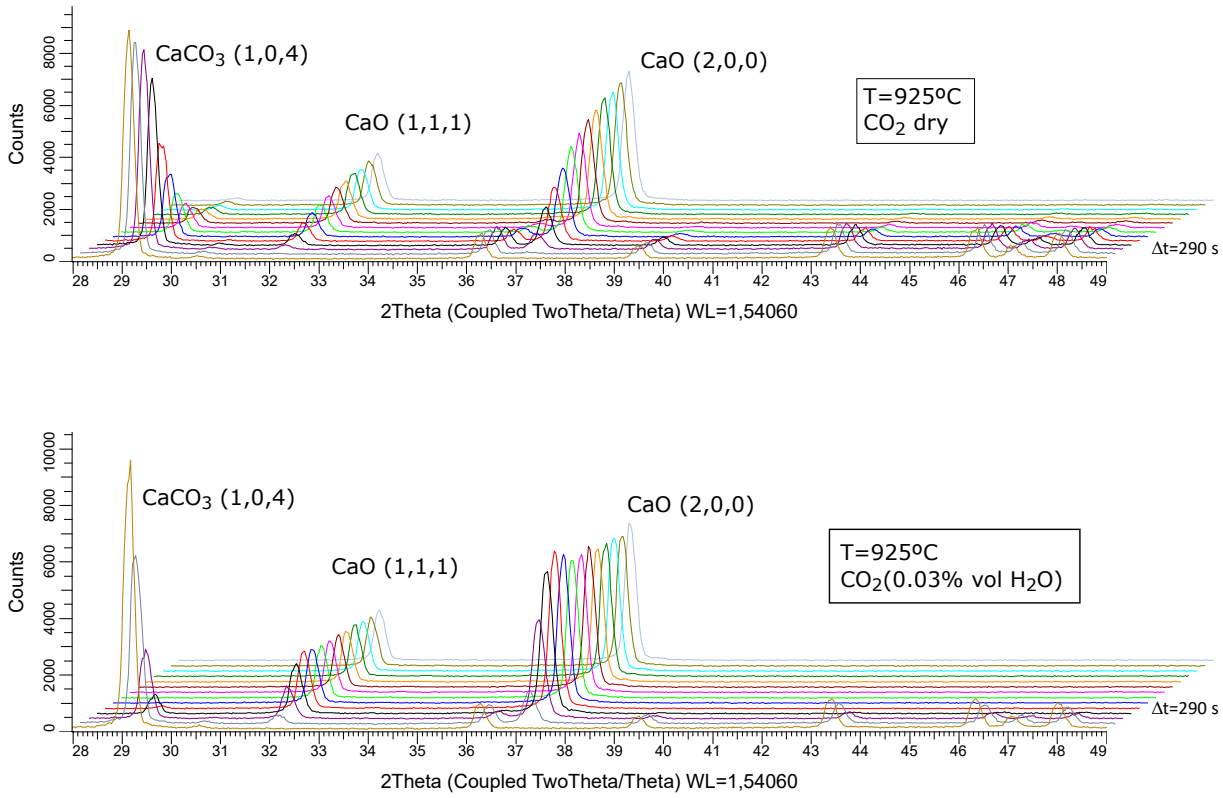

FIG. 6: Segments of the diffractograms recorded by in-situ XRD analysis during calcination of limestone at 925°C under dry and wet CO_2 (0.03 vol% H_2O). Main Bragg peaks of calcite ($CaCO_3$: Rombo.H.axes, space group $R\bar{3}c$ (163)) and lime (CaO: Cubic, space group $Fm\bar{3}m$ (225)) are indicated.

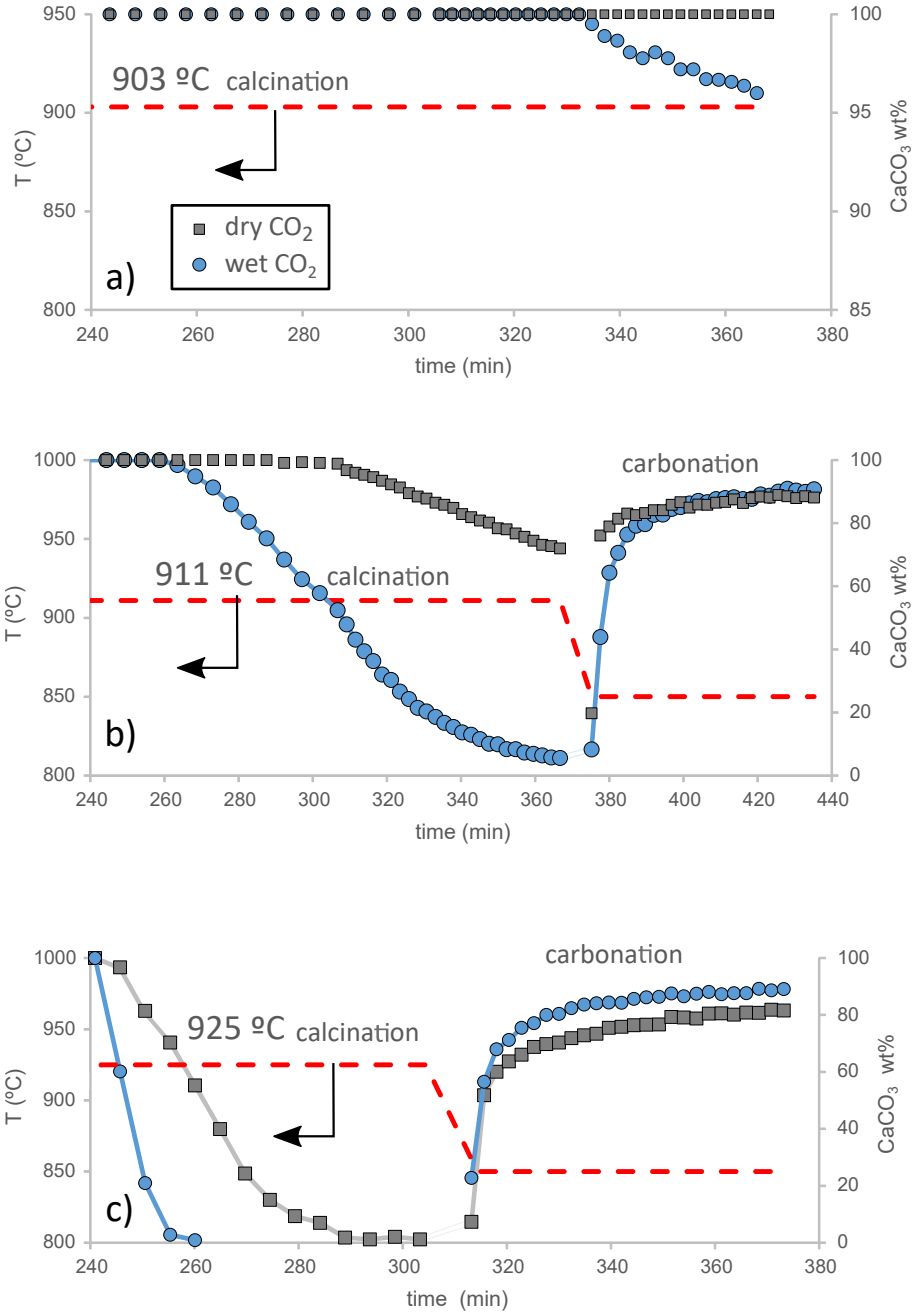

FIG. 7: Time evolution of temperature (left axis) and $CaCO_3$ wt% during calcination/carbonation tests carried out under dry and wet CO_2 at 903°C (a), 911°C (b), and 925°C (c).

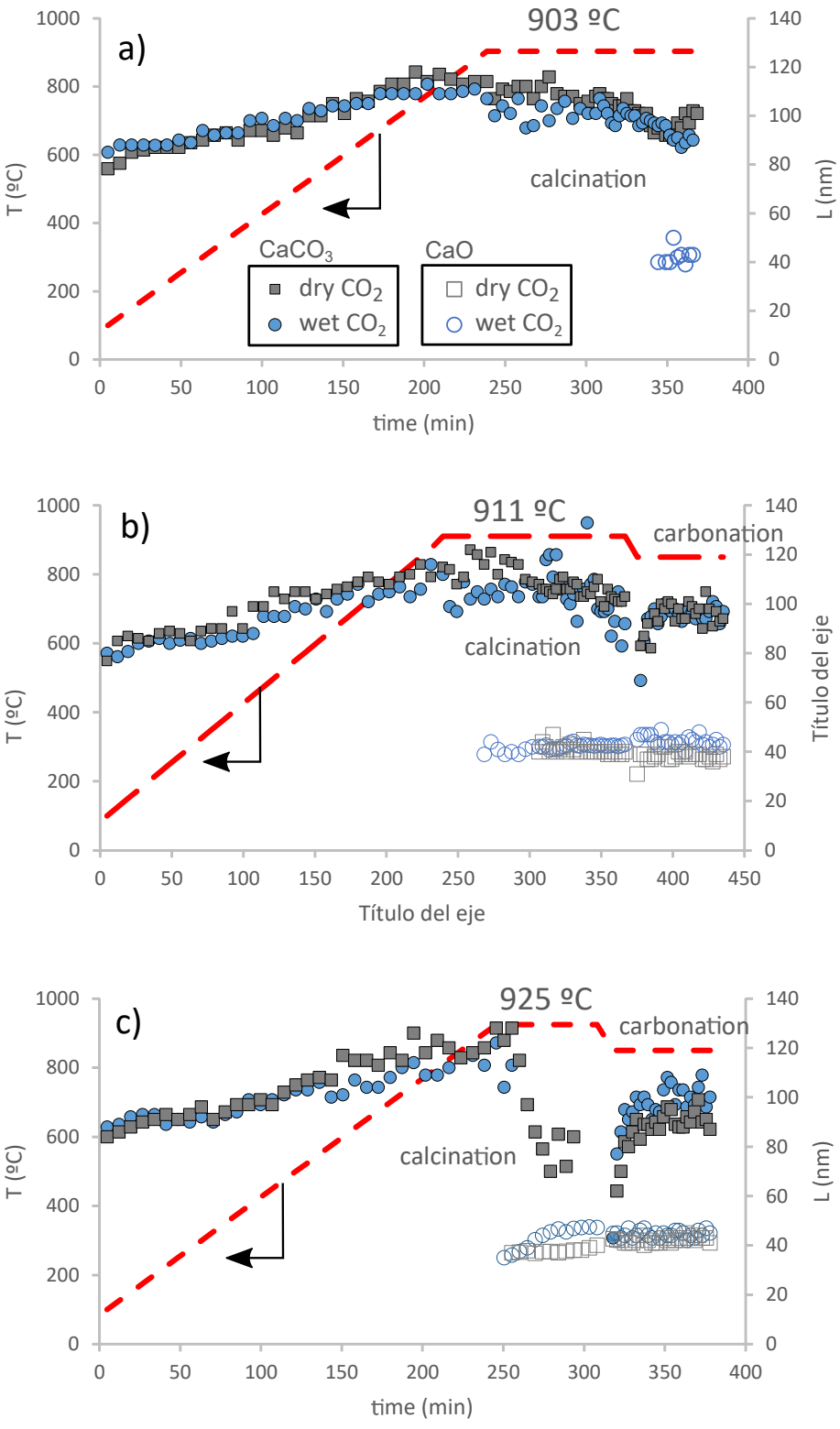

FIG. 8: Time evolution of temperature (left axis) and crystallite size (right axis) of $CaCO_3$ and CaO during calcination/carbonation tests carried out under dry and wet CO_2 at 903°C (a), 911°C (b), and 925°C (c).

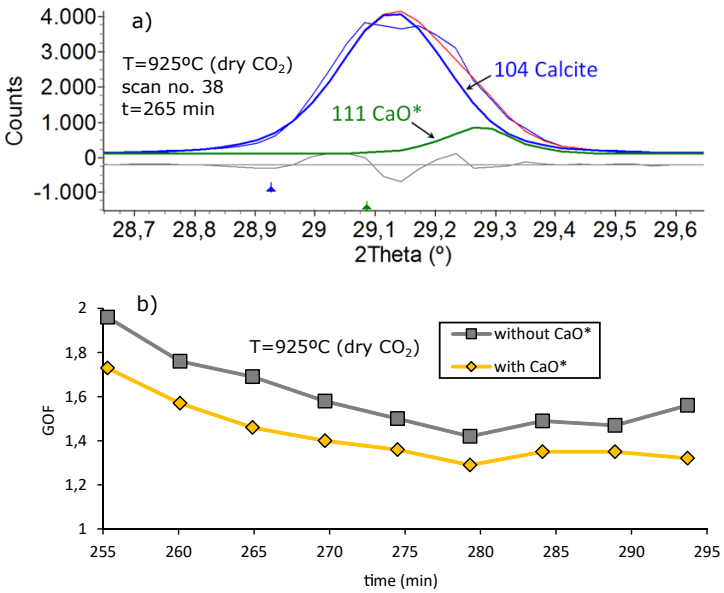

FIG. 9: a) Main Bragg reflection peak of calcite recorded (blue thin line) at scan 38 (t=265 min) during calcination under dry CO_2 (T=925°C), peak obtained from the best Rietveld fit (red thin line), which includes the contribution of calcite (blue thick line, 56.8% wt content) and CaO* (green line, 4.2% wt content) reflection peaks. b) Goodness-of-fit parameter obtained for the Rietveld best fits to experimentally recorded XRD patterns with and without taking into consideration the presence of the metastable CaO* phase during calcination under dry CO_2 (T=925°C).

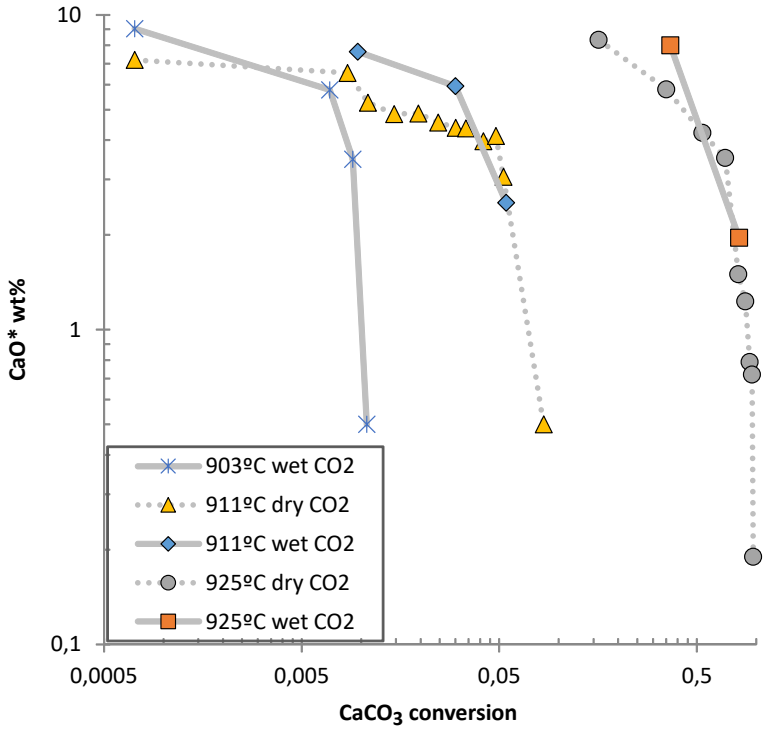

FIG. 10: Time evolution of CaO* wt% as a function of $CaCO_3$ conversion during calcination under dry and wet (0.03% wt H_2O) CO_2 at diverse temperatures as indicated (calculated by means of a Rietveld quantitative analysis).